

Strong-Field Scattering of Two Black Holes: Numerics Versus Analytics

Thibault Damour¹, Federico Guercilena^{2,3}, Ian Hinder², Seth Hopper², Alessandro Nagar¹, and Luciano Rezzolla^{3,2}

¹*Institut des Hautes Etudes Scientifiques, 91440 Bures-sur-Yvette, France*

²*Max-Planck-Institut für Gravitationsphysik, Albert-Einstein-Institut,
Am Mühlenberg 1, D-14476 Golm, Germany and*

³*Institut für Theoretische Physik, Max-von-Laue-Str. 1, D-60438 Frankfurt am Main, Germany*

(Dated: August 5, 2018)

We probe the gravitational interaction of two black holes in the strong-field regime by computing the scattering angle χ of hyperbolic-like, close binary-black-hole encounters as a function of the impact parameter. The fully general-relativistic result from numerical relativity is compared to two analytic approximations: post-Newtonian theory and the effective-one-body formalism. As the impact parameter decreases, so that black holes pass within a few times their Schwarzschild radii, we find that the post-Newtonian prediction becomes quite inaccurate, while the effective-one-body one keeps showing a good agreement with numerical results. Because we have explored a regime which is very different from the one considered so far with binaries in quasi-circular orbits, our results open a new avenue to improve analytic representations of the general-relativistic two-body Hamiltonian.

Introduction— Historically, elastic scattering experiments have been an essential tool to explore fundamental interactions in nature. Following this tradition, we have performed systematic numerical experiments exploring the gravitational interaction of two black holes (BHs) in a regime where strong-field effects become important. In this *Letter* we report on the first numerical-relativity (NR) computation of the gauge-invariant dynamical relation between the (center of mass) *scattering angle* χ of close binary-black-hole (BBH) encounters and the energy E and angular momentum J of the system. Differently from what has been done in previous works [1–6], which have looked at the *strongly inelastic* collision of two BHs leading to immediate (or prompt) merger, we here concentrate on what is an essentially (hyperbolic-like) *elastic* scattering.

More specifically, we study a set of configurations in which two equal-mass, nonspinning BHs start at large separations $\sim 100 GM/c^2$ with mildly relativistic individual velocities $|v_1|/c = |v_2|/c \approx 0.21$, approach each other within a few times their Schwarzschild radii, and then separate again towards infinity. By varying the initial angular momentum (or, equivalently, the impact parameter) we explore a large range of scattering angles from 70.7 degrees up to 305.8 degrees. We then compare the value of χ determined from NR to several analytical estimates: post-Newtonian (PN) theory and the effective-one-body (EOB) formalism [7–9], finding that PN becomes inaccurate for small values of the impact parameter, while EOB continues to show good agreement.

Numerical-relativity simulations— The simulations were performed using the open-source Einstein Toolkit [10] within the Cactus [11] framework, using the McLachlan [12] evolution code and 8th-order spatial finite differencing. The computational domain extends to $400 M$ in units in which $G = c = 1$, and outgoing radiative boundary conditions are used at the outer boundary. Here $M = m_1 + m_2$ where $m_1 = m_2$ is the

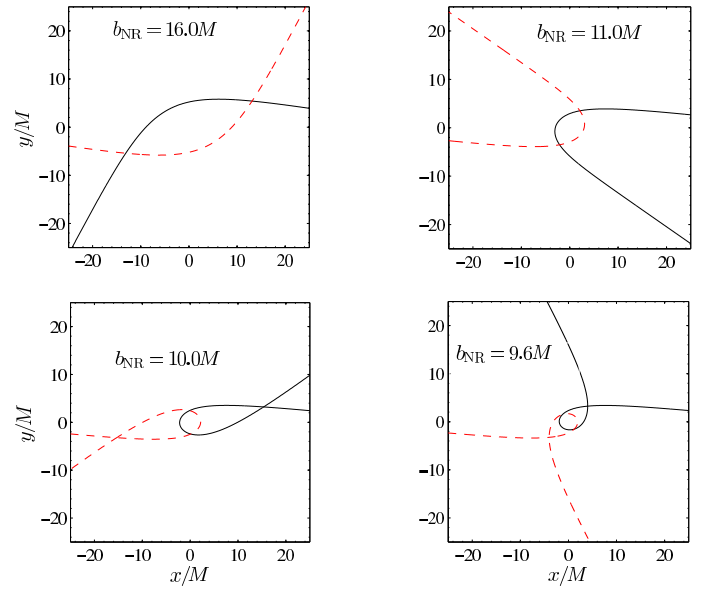


FIG. 1. Coordinate trajectories of the two BHs in hyperbolic-like encounters for four selected values of the impact parameter b_{NR} .

mass of each BH, as determined from the apparent horizons using the AHFinderDirect [13] code. The domain is discretised with a Cartesian numerical grid and 7 levels of box-in-box grid refinement around each BH provided by the adaptive-mesh-refinement code Carpet [14]. The refined regions track the BHs and have a finest grid spacing of $h = 0.025 M$ (low resolution) and $h = 0.017 M$ (high resolution).

Initial data of the Bowen-York form is constructed using the TwoPunctures [15] code. The BHs start on the x -axis with initial positions designated by $\pm X$ and initial momenta $(p_x, p_y, p_z) = \pm |\vec{p}|(-\sqrt{1 - (b_{\text{NR}}/(2X))^2}, b_{\text{NR}}/(2X), 0)$. Here b_{NR} is the NR “impact parameter”, which is related to the ADM an-

TABLE I. From left to right, the columns report: the NR “impact parameter”, the initial energy, the initial angular momentum, the gravitational-wave energy and angular-momentum losses.

b_{NR}/M	$E_{\text{in}}^{\text{NR}}/M$	$J_{\text{in}}^{\text{NR}}/M^2$	$\Delta E^{\text{NR}}/M$	$\Delta J^{\text{NR}}/M^2$
9.6	1.0225555(50)	1.099652(36)	0.01946(17)	0.17007(89)
9.8	1.0225722(50)	1.122598(37)	0.01407(10)	0.1380(14)
10.0	1.0225791(50)	1.145523(38)	0.010734(75)	0.1164(14)
10.6	1.0225870(50)	1.214273(40)	0.005644(38)	0.076920(80)
11.0	1.0225884(50)	1.260098(41)	0.003995(27)	0.06163(53)
12.0	1.0225907(50)	1.374658(45)	0.001980(13)	0.04022(53)
13.0	1.0225924(50)	1.489217(48)	0.0011337(90)	0.029533(53)
14.0	1.0225931(50)	1.603774(52)	0.0007108(77)	0.02325(47)
15.0	1.0225938(50)	1.718331(55)	0.0004753(75)	0.01914(76)
16.0	1.0225932(50)	1.832883(58)	0.0003338(77)	0.0162(11)

gular momentum via $J_{\text{ADM}} = 2X|p_y| = |\vec{p}| b_{\text{NR}}$. For all the simulations we use $|\vec{p}| = 0.11456439 M$, $X = 50 M$; more information on the 10 initial configurations is collected in Table I. Since these configurations vary only in the direction of the initial momentum, the ADM energy, E_{ADM} , of each spacetime is nearly the same ($E_{\text{ADM}} - M \approx 2.26 \times 10^{-2} M$), while the angular momentum $J_{\text{ADM}} = |\vec{p}| b_{\text{NR}}$ is proportional to b_{NR} . For our comparisons we are actually interested in the “initial” energy and angular momentum left after the burst of spurious radiation present in the initial data. These quantities, that we indicate as $(E_{\text{in}}^{\text{NR}}, J_{\text{in}}^{\text{NR}})$, differ fractionally by only 10^{-5} from $(E_{\text{ADM}}, J_{\text{ADM}})$ and are listed in Table I.

To ease the analytic computations of the scattering angle we have also measured the total energy, ΔE^{NR} , and angular momentum, ΔJ^{NR} , radiated in gravitational waves during the scattering event. We obtain these quantities by first computing the multipolar modes (up to $\ell = 8$) of the Weyl scalar Ψ_4 at several finite radii. At each radius we perform time-domain integrations of these moments and sum them to obtain ΔE^{NR} and ΔJ^{NR} . The resulting finite-radius values of ΔE^{NR} and ΔJ^{NR} are then extrapolated to null infinity. We (over-)estimate the extrapolation error in these quantities as the difference in the extrapolated value and the value at the largest radius.

We track the motion of the BHs using the Cartesian coordinate positions of the punctures which we convert to polar coordinates (r, φ) . Treating the incoming $\varphi_{\text{in}}(r)$ and outgoing $\varphi_{\text{out}}(r)$ paths separately, we extrapolate $\varphi_{\text{in,out}}(r)$ as $r \rightarrow \infty$ by fitting each of them to a polynomial of order n in $1/r$ to measure the two asymptotic angles $\varphi_{\text{in,out}}^\infty$ corresponding to a binary with infinite separation. The total scattering angle is then calculated as $\chi^{\text{NR}} \equiv \varphi_{\text{out}}^\infty - \varphi_{\text{in}}^\infty - \pi$. A range of (r, φ) must be

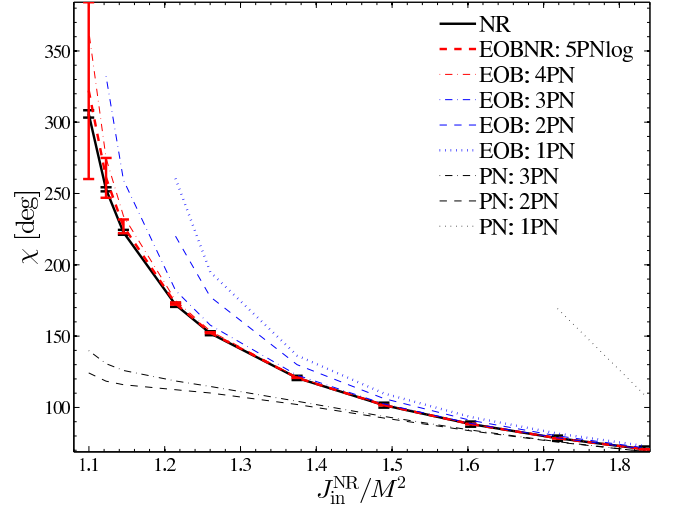


FIG. 2. Comparing the NR scattering angle with various EOB and PN predictions. NR data and the state-of-the-art EOB model agree within their respective error bars.

chosen to perform the polynomial fitting and compute $\varphi_{\text{in,out}}^\infty$. For the incoming and outgoing paths we extrapolate from $r \in [18.75, 75] M$ and $[25, 100] M$, respectively. With this choice, we extrapolate over a range in $1/r$ that is $1/4$ the size of the data we use for the fitting. Our least-squares fitting method employs a singular-value decomposition (SVD) which drops singular values smaller than a threshold (chosen to be 10^{-13} times the maximum singular value). We then choose the polynomial order n as the largest for which the SVD threshold allows variations in the constant term. We take as our estimate of the extrapolation error the maximum difference between the extrapolant at order n and the extrapolant at all orders between 1 and $n - 1$. We have tested that this error estimate is robust with respect to variations in the details of the extrapolation method. We expect that the extrapolated scattering angle will be insensitive to the details of the spatial gauge conditions employed due to their symmetry-seeking nature and the fact that the region between the far-separated BHs is approximately Minkowskian.

We estimate our finite-difference error in χ , ΔE^{NR} , and ΔJ^{NR} by performing each simulation with two different resolutions and (conservatively) assuming 4th-order convergence. The total error estimates, as shown in Table I, are computed by adding the finite-difference and extrapolation errors in quadrature. Note that we also explored other sources of error (e.g., the effect of finite initial separation and the choice of how much data to use in the fitting), but found that these were all much smaller.

EOB and PN analytic computations of χ and comparison with NR results— From the analytical relativity (AR) point of view, the scattering angle depends on

TABLE II. NR, EOB and PN estimates of the scattering angle χ at different PN orders. Angles are measured in degrees.

b_{NR}/M	$\hat{r}_{\text{min}}^{\text{EOB}}$	χ^{NR}	$\chi_{5\text{PNlog}}^{\text{EOBNR}}$	$\chi_{4\text{PN}}^{\text{EOB}}$	$\chi_{3\text{PN}}^{\text{EOB}}$	$\chi_{2\text{PN}}^{\text{EOB}}$	$\chi_{1\text{PN}}^{\text{EOB}}$	$\chi_{3\text{PN}}^{\text{PN}}$	$\chi_{2\text{PN}}^{\text{PN}}$	$\chi_{1\text{PN}}^{\text{PN}}$
9.6	3.3	305.8(2.6)	322(62)	364.29	139.9	124.2	...
9.8	3.7	253.0(1.4)	261(14)	274.92	332.24	131(2)	118.46	...
10.0	4.0	222.9(1.7)	227(5)	234.26	259.46	126(1)	115.89	...
10.6	4.8	172.0(1.4)	172.8(7)	174.98	182.09	220.11	260.53	118.5(3)	112.43	...
11.0	5.3	152.0(1.3)	152.4(3)	153.59	157.68	177.60	194.90	114.7(2)	110.14	...
12.0	6.5	120.7(1.5)	120.77(6)	121.17	122.63	129.98	136.42	104.34(4)	102.06	...
13.0	7.6	101.6(1.7)	101.63(2)	101.80	102.48	106.20	109.80	93.69(2)	92.54	...
14.0	8.6	88.3(1.8)	88.348(8)	88.43	88.80	90.95	93.30	84.111(7)	83.55	...
15.0	9.7	78.4(1.8)	78.427(4)	78.47	78.69	80.03	81.699	75.962(3)	75.71	169.298
16.0	10.8	70.7(1.9)	70.666(2)	70.69	70.84	71.71	72.951	69.122(2)	69.03	108.894

the full equations of motion, including both conservative (Hamiltonian H) and radiation-reaction ($\mathcal{F}_{\text{rad reac}}$) effects. The current AR knowledge of $\mathcal{F}_{\text{rad reac}}$ along general (non-quasi-circular) motions [16] is less complete than that of H and cannot be used for accurate NR/AR comparisons. However, it has been recently pointed out [16] that, when neglecting terms quadratic in $\mathcal{F}_{\text{rad reac}}$ (i.e., of order $(v/c)^{10}$, where v is the velocity), the scattering angle χ can be analytically computed solely from the knowledge of the Hamiltonian H . More precisely, the AR approximation χ^{AR} is given by the value it would have in a conservative-dynamics scattering of a binary system whose energy and angular momentum are the *average* values between the incoming and outgoing states:

$$\chi^{\text{AR}} = \chi^{(\text{conservative})}(\bar{E}, \bar{J}), \quad (1)$$

where $\bar{E} \equiv (E_{\text{in}} + E_{\text{out}})/2$ and $\bar{J} \equiv (J_{\text{in}} + J_{\text{out}})/2$. Using the NR measures of the radiative NR losses $\Delta E^{\text{NR}} = E_{\text{in}}^{\text{NR}} - E_{\text{out}}^{\text{NR}}$, $\Delta J^{\text{NR}} = J_{\text{in}}^{\text{NR}} - J_{\text{out}}^{\text{NR}}$, we have $\bar{E} = E_{\text{in}}^{\text{NR}} - \Delta E^{\text{NR}}/2$ and $\bar{J} = J_{\text{in}}^{\text{NR}} - \Delta J^{\text{NR}}/2$.

We compute χ^{AR} using various EOB and PN Hamiltonians. In all cases, we numerically integrate the equations of motion from an initial separation $r_0 = 10000 M$ up to a comparable final separation, and compute $\chi^{\text{AR}} \equiv \varphi_{\text{final}} - \varphi_0 - \pi$. In the following we denote $\mu \equiv m_1 m_2 / M$, $\nu = \mu / M$, $j \equiv p_\varphi \equiv J / (M\mu)$, and $u \equiv M/r$.

The EOB conservative binary dynamics is completely encoded in two functions $A(u; \nu)$ and $B(u; \nu)$. The radial interaction potential A is a ν -deformed generalization of the Schwarzschild potential $A_{\text{Schw}} \equiv 1 - 2M/r = 1 - 2u$. The potentials A and B feed into the EOB Hamiltonian $H_{\text{EOB}}(r, p_\varphi, p_r) \equiv M \sqrt{1 + 2\nu (H_{\text{eff}}/\mu - 1)}$, where $H_{\text{eff}} = \mu \sqrt{A(1 + j^2 u^2 + 2\nu(4 - 3\nu)u^2 p_{r*}^4) + p_{r*}^2}$. Here $p_{r*} \equiv \sqrt{A/B} p_r$ is a tortoise version of the μ -rescaled radial momentum $p_r \equiv P_r/\mu$.

Currently, the analytically most complete (5PN with logs), NR-calibrated version of A [17] is defined as the Padé approximant $P_5^1(A_{5\text{PNlog}}^{\text{Taylor}})$ with $A_{5\text{PNlog}}^{\text{Taylor}} \equiv 1 -$

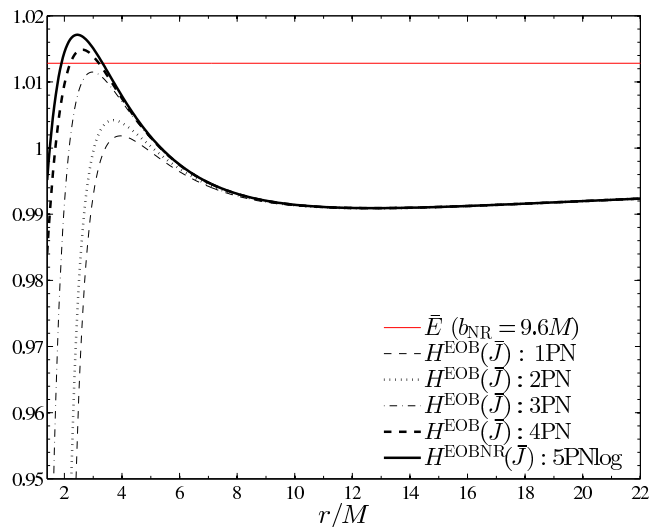


FIG. 3. EOB effective potentials $H_{\text{EOB}}(r, \bar{J}, p_r = 0)$ at various PN approximations. The values $(\bar{E}, \bar{J}) = (E_{\text{in}} - \frac{1}{2}\Delta E^{\text{NR}}, J_{\text{in}}^{\text{NR}} - \frac{1}{2}\Delta J^{\text{NR}})$ correspond, in Table I, to $b_{\text{NR}} = 9.6 M$. The EOB motion corresponds to a particle starting at large r with negative radial momentum p_r^0 and moving towards the left at constant energy \bar{E} . Note that 1PN, 2PN and 3PN EOB models predict plunge instead of scattering.

$2u + 2\nu u^2 + \nu a_4 u^3 + \nu(a_5^c(\nu) + a_5^{\log} \log u)u^4 + \nu(a_6^c(\nu) + a_6^{\log} \log u)u^5$. Here $a_5^c \equiv a_5^{\text{eff}} = 23.5$ and $a_6^c \equiv a_6^{\text{eff}} = (-110.5 + 129(1 - 4\nu))\sqrt{1 - (1.5 \times 10^{-5})/(\nu - 0.26)^2}$. The analytically most complete version of B is defined through $\bar{D} \equiv 1/(AB)$, with $\bar{D}_{4\text{PN}} = 1 + \nu [\bar{d}_2 u^2 + \bar{d}_3(\nu)u^3 + (\bar{d}_4^c + \bar{d}_4^{\log} \log u)u^4]$. Here, contrary to [17], which used the 3PN-accurate \bar{D} function, we use the above 4PN-accurate version with $\bar{d}_4^c = 226$ [18, 19] and $\bar{d}_4^{\log} = 592/15$ [18–20]. Hereafter we will refer to this state-of-the-art EOB model as “EOBNR_{5PNlog}”. We start the integration of the EOB equations of motion

with $j_0 = \bar{J}/(M\mu)$ and $p_{r_*}^0$ obtained by solving the equation $\bar{E} = H_{\text{EOB}}(r_0, j_0, p_{r_*}^0)$. The gauge-invariant scattering angle $\chi_{5\text{PNlog}}^{\text{EOBNR}}(\bar{E}, \bar{J})$ obtained from this integration is given in the fourth column in Table II, to be compared to the corresponding NR results (third column). The agreement between these values of χ is remarkably good. The fractional disagreements are equal to: 0.048% for the largest impact parameter ($b_{\text{NR}} = 16M$); 1.8% for $b_{\text{NR}} = 10M$ and 5.3% for the smallest impact parameter, $b_{\text{NR}} = 9.6M$ (which corresponds to a closest EOB relative distance $r_{\text{min}}^{\text{EOB}} = 3.3M$) [see Fig. 2].

We (over-)estimate a two-sided uncertainty on $\chi_{5\text{PNlog}}^{\text{EOBNR}}$ $\sigma_\chi \equiv \pm \frac{1}{2}[\langle \chi(E, J) \rangle - \chi(\bar{E}, \bar{J})]$ by comparing $\chi(\bar{E}, \bar{J})$ to the average value $\langle \chi \rangle = \frac{1}{2}(\chi_{\text{in}} + \chi_{\text{out}})$ where $\chi_{\text{in}} \equiv \chi(E_{\text{in}}, J_{\text{in}})$ and $\chi_{\text{out}} \equiv \chi(E_{\text{out}}, J_{\text{out}})$. This uncertainty is given in parentheses on the last two digits in Table II. [In the case $b_{\text{NR}} = 9.6M$, E_{out} is so small that one cannot use this procedure. In that case we estimate an analytical uncertainty from the curvature of the function $\chi(E, J)$ around (\bar{E}, \bar{J})]. Note that, as is evident in Fig. 2, if we consider the combined uncertainties on χ , the NR and EOBNR_{5PNlog} results are fully compatible for the entire examined parameter space.

To probe the sensitivity of this NR/EOB agreement on the precise structure of the EOB Hamiltonian, we analyze the effects of replacing the 5PN-accurate A and the 4PN-accurate \bar{D} potentials used in EOBNR_{5PNlog} by potentials of lower PN accuracy. We denote by EOB _{n PN} an EOB Hamiltonian defined by truncating the A and \bar{D} potentials to their n PN accuracy. The result of the corresponding analytical computations of χ are listed in Table II. Note that as we lessen the PN accuracy of the EOB Hamiltonian, the disagreement in χ increases monotonically (see Fig. 2). The empty slots in Table II correspond to configurations where the peak of the EOB effective potential is lower than \bar{E} , so that the analytical evolution leads to an immediate plunge (see Fig. 3).

Finally, we explored the sensitivity of the NR/AR comparison on the resummation procedure built into the EOB formalism, by computing the predictions for χ made by the *nonresummed* PN-expanded Hamiltonian. At 3PN accuracy, this (center-of-mass) Hamiltonian (in ADM coordinates) is a polynomial with 24 terms of the form $(H - M)/\mu \sim \frac{1}{2}p^2 - 1/r + c^{-2}(p^4 + p^2/r + 1/r^2) + c^{-4}(p^8 + \dots + 1/r^4) + c^{-6}(p^{10} + \dots + 1/r^4)$ (see [21, 22]). The result of computing χ (following the same procedure as above) from this 3PN Hamiltonian is listed in the 9th column of Table II. In addition, the result of considering 2PN and 1PN truncations of this Hamiltonian is included in the table. Several conclusions can be drawn from this comparison. First, for most values of the impact parameter b_{NR} the PN_{3PN}/NR disagreement is significantly larger than the corresponding EOB_{3PN}/NR disagreement (see Fig. 2). For instance, for $b_{\text{NR}} = 16M$, PN_{3PN} and NR disagree by -2.2% , while EOB_{3PN} and NR disagree by 0.20% ; and for $b_{\text{NR}} = 10.6M$, PN_{3PN} and NR disagree by

-31% , while EOB_{3PN} and NR disagree by $+5.9\%$. Note also the sizable difference between the predictions made by the 1PN-accurate PN-expanded Hamiltonian and the 1PN-accurate PN-resummed EOB Hamiltonian: e.g., for $b_{\text{NR}} = 16M$, the PN prediction disagrees with NR by $+54\%$ while the EOB disagreement is just $+3.2\%$.

Conclusions— We have performed the first numerical computation of the scattering angle χ of nonspinning, equal-mass BBH encounters varying the impact parameter while keeping essentially fixed the incoming energy. The range of explored impact parameter is such that the scattering angle varies between 70.7 and 305.8 degrees. Correspondingly, the closest distance of approach of the two BHs (in EOB coordinates) was found to vary between $10.8M$ and $3.3M$, indicating that we are indeed exploring the strong-field dynamics of the BHs. We have compared the NR data to two different analytical approaches to describing the orbital dynamics of BBHs: PN theory and the EOB formalism. Our main finding is that, as the impact parameter b_{NR} decreases, the PN predictions become quite inaccurate (by more than a factor 2) while the NR-calibrated EOB predictions keep agreeing with NR within their combined error bars. This NR/EOB agreement is remarkable since the configurations considered here explore a dynamical regime, in the (E, J) plane, which is very different from the quasi-circular configurations used for the calibration of the EOB model. Note also how the uncalibrated, purely analytical, EOB models monotonically approach the NR results as their PN accuracy is increased (see Fig. 2).

Overall, our study opens a new avenue for extracting from NR simulations nonperturbative information to complete the EOB formalism. In particular NR scattering experiments for small impact parameters allow one to probe the height and shape of the EOB effective energy potential very close to its peak, i.e., for BH separations of the order of $3M$.

SH, IH, and LR thank Abraham Harte for helpful discussions. The computations were performed on the Datura cluster at the AEI and on the XSEDE network (allocation TG-MCA02N014). This work was supported in part by the DFG grant SFB/Transregio 7 “Gravitational-Wave Astronomy”.

-
- [1] F. Pretorius and D. Khurana, *Class.Quant.Grav.* **24**, S83 (2007).
 - [2] M. Shibata, H. Okawa, and T. Yamamoto, *Phys.Rev.* **D78**, 101501 (2008).
 - [3] U. Sperhake, V. Cardoso, F. Pretorius, E. Berti, and J. A. Gonzalez, *Phys.Rev.Lett.* **101**, 161101 (2008).
 - [4] U. Sperhake, V. Cardoso, F. Pretorius, E. Berti, T. Hinderer, *et al.*, *Phys.Rev.Lett.* **103**, 131102 (2009).
 - [5] H. Witek, M. Zilhao, L. Gualtieri, V. Cardoso, C. Herdeiro, *et al.*, *Phys.Rev.* **D82**, 104014 (2010).

- [6] U. Sperhake, E. Berti, V. Cardoso, and F. Pretorius, *Phys.Rev.Lett.* **111**, 041101 (2013).
- [7] A. Buonanno and T. Damour, *Phys. Rev.* **D59**, 084006 (1999).
- [8] A. Buonanno and T. Damour, *Phys. Rev.* **D62**, 064015 (2000).
- [9] T. Damour, P. Jaranowski, and G. Schaefer, *Phys. Rev.* **D62**, 084011 (2000).
- [10] F. Löffler, J. Faber, E. Bentivegna, T. Bode, P. Diener, *et al.*, *Class.Quant.Grav.* **29**, 115001 (2012).
- [11] Cactus developers, “Cactus Computational Toolkit,” .
- [12] J. D. Brown, P. Diener, O. Sarbach, E. Schnetter, and M. Tiglio, *Phys. Rev. D* **79**, 044023 (2009).
- [13] J. Thornburg, *Class. Quantum Grav.* **21**, 743 (2004).
- [14] E. Schnetter, S. H. Hawley, and I. Hawke, *Class. Quantum Grav.* **21**, 1465 (2004).
- [15] M. Ansorg, B. Brügmann, and W. Tichy, *Phys. Rev. D* **70**, 064011 (2004).
- [16] D. Bini and T. Damour, *Phys.Rev.* **D86**, 124012 (2012).
- [17] T. Damour, A. Nagar, and S. Bernuzzi, *Phys.Rev.* **D87**, 084035 (2013).
- [18] L. Barack, T. Damour, and N. Sago, *Phys.Rev.* **D82**, 084036 (2010).
- [19] E. Barausse, A. Buonanno, and A. Le Tiec, *Phys.Rev.* **D85**, 064010 (2012).
- [20] L. Blanchet, S. L. Detweiler, A. Le Tiec, and B. F. Whiting, *Phys.Rev.* **D81**, 084033 (2010).
- [21] P. Jaranowski and G. Schaefer, *Phys.Rev.* **D57**, 7274 (1998).
- [22] T. Damour, P. Jaranowski, and G. Schaefer, *Phys.Lett.* **B513**, 147 (2001).